Engineering Transactions, **74**(1): 69–84, 2026, https://doi.org/10.24423/engtrans.2025.3603
Institute of Fundamental Technological Research Polish Academy of Sciences (IPPT PAN)
Université de Lorraine • Poznan University of Technology

Research Paper

A Prime-Number/Uniform Angular Distribution Criterion for Blade Vibration Reduction

Yong Li, Yaao Di, Wenzheng Dong, Fangxiang Yin, Yihao Yin, Shanling Han*

College of Mechanical and Electronic Engineering, Shandong University of Science and Technology
Qingdao, China

*Corresponding Author: 15806673969@163.com

Currently, the vibration noise of casting cleaning equipment exceeds 95 dB, which not only shortens the equipment's service life but also jeopardizes workers' health. The primary cause lies in the resonance tendency resulting from an uneven distribution of blades in the shot-blasting device. In this paper, a prime-number/uniform angular distribution criterion and a dynamic balance elimination relationship are established to minimize resonance coupling while accounting for the internal characteristics of the shot-blasting device and blade assembly. Subsequently, a shot-blasting device with seven prime-number angular front-curved blades was designed and fabricated, and the dynamic imbalance caused by uneven blade distribution was compensated for by drilling. We employed the discrete element method to evaluate projectile velocity and stability. The results indicate that the shot velocity reaches a maximum of 75 m/s, with fluctuations within 4 m/s. After reaching 0.24 s, particles accelerated by the shot-blasting device achieve relative stability. Finally, vibration data acquired at a sampling frequency of 10 Ksps demonstrates that noise levels are reduced from 97 dB (traditional structure) to 93.3 dB (new model). This new criterion for shot-blasting machine models mitigates operational vibration while enhancing working conditions and improving overall stability and system reliability.

Keywords: shot-blasting machine, vibration-induced noise, structural optimization, prime-number/uniform angular distribution criterion, shot-blasting device with seven prime-number angular front-curved blades.

1. Introduction

As a surface treatment equipment, the shot-blasting machine finds extensive application across various industries. However, operational vibration and noise issues associated with this machinery significantly impact equipment performance, personnel well-being, and environmental conditions [1]. The vibration

frequency can be decomposed into the fundamental frequency and its second harmonic using Fourier series analysis [2–5]. The fundamental frequency for uniformly distributed shot-blasting blades corresponds to the fundamental blade-passing frequency (BPF). Resonance occurs when either the fundamental frequency or the second harmonic ($2 \times$ BPF) of the blade coincides with the natural frequency of the shot-blasting device [6–9]. Due to the periodic nature of blade rotation, uniformly distributed blades are more likely to induce resonance by matching the system's natural frequency, thereby increasing the associated risk.

Using the studies from other industries, some researchers have designed blades as a means of reducing equipment noise. Luo *et al.* [10] reported that a non-uniformly arranged seven-blade fan exhibits distinctive noise characteristics during tests. In comparison with a uniformly arranged fan, the noise characteristics of a non-uniformly arranged fan display a broader harmonic distribution and a reduced disparity between discrete and broadband noise. It is evident that incorporating non-uniform blade arrangements offer certain advantages in vibration and noise reduction; however, prime-number angular designs have been applied only in one instance within other industries and lacks a general design principle. In this study, non-uniform blade design is incorporated into shot-blasting machines and a prime-number/uniform angular distribution criterion is proposed for a new type of shot blaster. Zhang *et al.* [11] analyzed the blades of shot-blasting machines and found that rectangular blades can alleviate stress concentration, providing valuable guidance for improving reliability and extending service life of these machines. Currently, although blade optimization has been employed to reduce stress concentration, blade arrangement has received little attention, and improvements in vibration-induced noise reduction for shot-blasting machines remain insufficient.

The objective of this study is to provide theoretical support for optimizing the design of a shot-blasting device through of vibration signal analysis and the establishment of blade selection criteria. The optimization design is conducted based on a prime-number/uniform angular distribution vibration reduction criterion, leading to the proposal of a shot-blasting device model incorporating seven prime-number angular front-curved blades. Subsequent analysis of object velocity and stability during the ejection process is conducted using the discrete element method [12]. By calculating parameters such as particle velocity changes, we can evaluate the ejection stability of the device. To address the imbalance caused by uneven blade distribution, perforations are introduced in the impeller disk to adjust the rotating dynamic balance of the shot-blasting device. Finally, vibration signal acquisition equipment is used to compare vibration signal characteristics between the newly designed shot blaster and traditional models, thereby verifying the performance advantages of the proposed criterion-based impeller structure.

2. Establishment of the prime-number/uniform angular distribution criterion for shot blasting

The design of a shot-blasting device not only requires blade shape improvement, but also optimization of the impeller body design to reduce resonance effects [13–17]. Vibration signal analysis reveals resonance between the motor and the impeller body, indicating the necessity for optimization of the shot-blasting device design. A key measure is to optimize the blade distribution angles and establish a prime-number/uniform angular distribution criterion for the blades. The criterion is defined through the following steps:

- calculate the desired uniform angular spacing based on the number of blades,
- select prime-number angular positions within the range of 1° to 361° to address centroid offset caused by blade arrangement,
- determine a set of angles with minimal standard deviation using Eq. (2.1).

This criterion aids in selecting blade mass angles close to the ideal uniform angle, thereby effectively enhancing the system's resonance frequency, reducing vibration and noise resulting from resonance, and improving the mechanical equipment's operational smoothness.

The prime-number/uniform angular distribution criterion relationship is derived from the standard deviation formula:

$$S = \sqrt{\frac{\sum_{i=1}^{n} \left(\operatorname{wrap}\left(\theta_i + \varphi\right) - \frac{360^\circ}{n} \cdot i \right)^2}{n}}, \tag{2.1}$$

where S is the standard deviation, θ_i is the i-th prime-number angular position (in degrees), n is the number of blades in the shot-blasting machine, φ is the phase shift, with $\varphi \in [0^\circ, 360^\circ/n)$. To account for the cyclic nature of $[0^\circ, 360^\circ)$, differences are evaluated as minimum signed circular (wrapped) errors using $\operatorname{wrap}(x) = ((x + 180^\circ) \bmod 360^\circ) - 180^\circ$. By minimizing S with respect to φ, the uniformity of the blade distribution relative to an arbitrarily shifted uniform distribution can be assessed.

In practice, the majority of existing shot-blasting devices employ either six or eight blades, and the number of shot-blasting shafts is typically four. An imbalance in blade number can adversely affect both the distribution and number of smaller shafts. An excessive number of small shafts hampers ejection efficiency, whereas an insufficient number compromises the structural strength of the shot-blasting device. Accordingly, based on the proposed prime-number/uniform angular distribution criterion of the blade, this research opts for a specific case: a shot-blasting device with seven prime-number angular blades. Let $n = 7$, and

substitute it into the prime-number/uniform angular distribution criterion, as per established academic standards.

Consequently, an impeller body for a prime-number angular blade vibration-damping shot-blasting device is established. The utilization of prime-number angular positions reduces the likelihood of resonance with other components due to their unique distribution characteristics, as they do not share common factors with other excitation frequencies in the system.

Subsequently, the impeller model of the shot-blasting device is established. Since prime numbers do not share common factors with other numbers, the angular distribution using prime-number indexing can reduce the risk of resonance with other components. According to Eq. (2.1), when $\varphi \in [0^\circ, 360^\circ/7)$, the minimum standard deviation is obtained by applying a search step size of $\Delta\varphi = 0.1^\circ$, which enhances the precision of the results, while a longer search interval ensures the robustness of the calculation. The results show that at $\varphi = 14.7^\circ$, the optimal prime-number angular positions are 37°, 89°, 139°, 191°, 241°, 293°, and 347°, yielding a standard deviation $S \approx 0.99$. This represents the smallest standard deviation, indicating that the angular distribution of the blade positions is closest to an equidistant distribution, thus ensuring greater stability and reliability of the system.

In terms of geometric uniformity, S reflects the degree of angular distribution uniformity, with smaller values of S indicating better uniformity. However, completely equidistant distributions do not necessarily result in optimal dynamic performance. A perfectly uniform distribution concentrates excitation energy at the BPF and its harmonics, which could lead to resonance if these frequencies coincide with the system's natural frequencies. Therefore, the design criterion is not solely to minimize S, but rather achieve minimal S while simultaneously ensuring that dominant frequency orders are shifted to avoid resonance with the system's natural frequencies, thereby optimizing the system's stability and operational reliability.

To further mitigate resonance risk, a resonance risk index $R(\Theta)$ is introduced to assess the relative relationship between blade frequencies and the system's natural frequencies. The resonance risk index is calculated as follows:

$$R(\Theta) = \max_{h\in\mathcal{H}} \left| \frac{1}{n} \sum_{i=1}^{n} e^{jh\theta_i} \right|, \tag{2.2}$$

where $\mathcal{H}$ represents the set of critical frequency orders corresponding to the system's natural frequencies and h denotes the frequency order. In this study, $h = 1, 2, 3, 4, 8, 9$, covering the fundamental frequency and its harmonics. Here, θ_i represents the angular position of the i-th blade.

The parameter $R(\Theta)$ represents the resonance risk index, reflecting the relationship between excitation frequency of the blades and the system's natural

frequency. The value of $R(\Theta)$ indicates the degree of difference between excitation frequency and natural frequencies. A value of $R(\Theta)$ close to 0 suggests no resonance risk, while $R(\Theta)$ approaching 1 indicates a significant risk of resonance. The value of $R(\Theta)$ ranges from 0 to 1, with 0 indicating no resonance risk and 1 corresponding to a high resonance risk. If $R(\Theta)$ is less than 0.1, it indicates low resonance risk, and the system's frequency distribution is generally well aligned. Based on the above frequency analysis, the calculated value of $R(\Theta) = 0.0736$ suggests a low resonance risk and demonstrates the system's favorable frequency alignment, thus avoiding potential resonance problems.

The generated blade angles are all prime-number angular positions, and since they share no common factors, their multiples do not coincide. Due to the distinct nature of prime numbers, their distribution is 'uniform,' thereby avoiding synchronous resonance among the blades. For the seven blade angles $\theta_1, \theta_2, \theta_3, ..., \theta_7$, their relationship is defined by Eq. (2.3). If $\Delta\theta$ is a fixed value (e.g., uniformly distributed angles), the motion periods of the blades become synchronized, leading to resonance. However, if the blade angles are selected as prime-number angular positions (such as 37°, 89°, etc.), the multiples of these angular values do not overlap within the same cycle, thereby preventing resonance:

$$\theta_i = \theta_1 + i \cdot \Delta\theta \quad (i = 1, 2, ..., 7), \tag{2.3}$$

where θ_i is the angle of the i-th blade and $\Delta\theta$ is the angular difference between adjacent blades.

In rotating machinery, the angular distribution of blades is directly related to their vibration modes and frequencies. Each blade angle can be considered a vibration source associated with the rotational period. When the angular intervals between blades follow a regular pattern, vibrations from all blades may synchronize at specific rotational frequencies, leading to resonance. In contrast, blade angles exhibit a prime-number distribution to avoid repeated angular intervals and suppress resonance effectively prevents such synchronization. Due to the inherent disparities between prime numbers – such as their lack of common factors – their multiples do not coincide within the same rotational cycle. Consequently, blades positioned at distinct prime-number angular positions exhibit differentiated rotational frequencies, thereby suppressing resonance.

As shown in Table 1, the parameters of the shot-blasting machine during operation are listed. All blades are made from high-chromium cast iron and have uniform dimensions.

The unbalanced mass of the newly designed shot-blasting machine is subsequently determined by employing Eq. (2.4) to Eq. (2.6). The blade material is high-chromium cast iron, a density is $7.8 \times 10^3\,\mathrm{kg/m^3}$, and a mass is 0.0836 kg. The static equilibrium mass of each blade is calculated to be 11.1796 g. The gov-

Table 1. Material parameters for different components.

Component	Parameter	Numerical value
Steel pellet (cast steel)	Poisson's ratio	0.3
	Density [kg/m^3]	7.8×10^3
	Shear modulus [Pa]	8×10^{10}
Impeller body, directional sleeve, shot-dividing wheel, blades (all components are made of high-chromium cast iron)	Poisson's ratio	0.3
Impeller body	Density [kg/m^3]	7.8×10^3
	Shear modulus [Pa]	7.6×10^{10}
	Impeller body speed [rpm]	3000

erning equations for calculating the unbalanced mass and its orientation are as follows, leading to a conclusive result:

$$\begin{cases} (m_b r_b)_x = -\sum_{i=1}^{n} mr \cdot \cos(\theta_i), \\ (m_b r_b)_y = -\sum_{i=1}^{n} mr \cdot \sin(\theta_i), \end{cases} \tag{2.4}$$

$$\alpha_b = \arctan \frac{(m_b r_b)_y}{(m_b r_b)_x}, \tag{2.5}$$

$$m_b r_b = \sqrt{\left[(m_b r_b)_x^2 + (m_b r_b)_y^2\right]}, \tag{2.6}$$

where m_b is the equilibrium mass, r_b is the distance from the blade center of mass to the rotor center, m is the mass of a single blade, r is the distance from the blade center of mass to the edge of the main (secondary) disk, θ_i is the i-th blade angular position on the shot-blasting machine, n is the number of blades on the shot-blasting machine, and α_b is the phase angle.

We then applied a formula to calculate the dynamic balance of the shot-blasting blade. The eccentric mass for static balance is determined, and we measure the distanced from the centroid of the shot-blasting blade to the disk edges as 68 mm for the main disk, and 52.5 mm for the secondary disk. By applying Eq. (2.7) and Eq. (2.8), we determine that dynamic balance masses were calculated as 4.890 g for the main disk, and 6.309 g for the secondary disk:

$$m_i r_i = \frac{y_1 + y_2 - y_i}{y_1 + y_2} m_b r_b, \tag{2.7}$$

$$m_{bi} = \frac{m_i r_i}{r_{bi}}, \tag{2.8}$$

where $m_i r_i$ is the blade is assigned to a mass radius product on a disk $i = 1$ for the primary disk and $i = 2$ for the secondary disk, y_i is the distance between the blade's center of mass and the edge of the main (secondary) disk, m_{bi} is dynamic balance mass, r_{bi} is the distance from the center of mass of the dynamically balancing mass to the disk center.

After assembly, the impeller body is equipped with blades and subjected to unbalance detection on a dynamic balancing machine (as depicted in Fig. 1), with the machine parameters listed in Table 2. The rotational acceleration test of the impeller body is conducted using an electrical measurement system to quantify the unbalance. The obtained test results reveal that at 288°, the main disk exhibits an unbalance of 2.924 g, while the secondary disk shows an unbalance of 4.460 g at 272°; after rotation ceases, the main disk displays an unbalance of 2.918 g while the secondary disk shows an unbalance of 4.520 g.

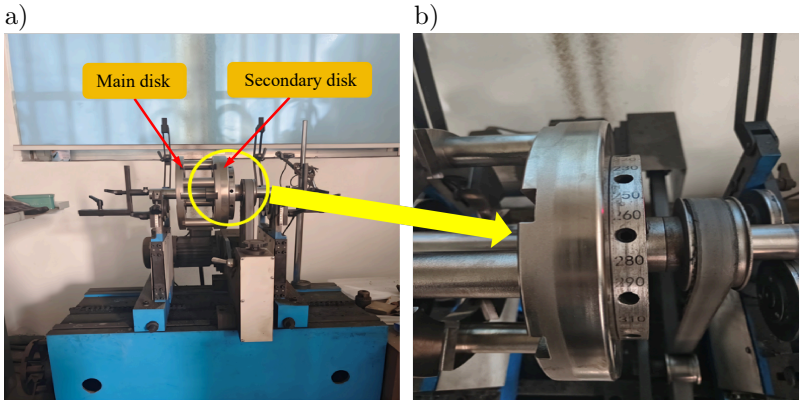

FIG. 1. Imbalance detection of the impeller body using a dynamic balancing machine (a), angle indicator on the dynamic balancing machine (b).

TABLE 2. Dynamic balancing machine parameters.

Parameter	Value
Maximum rotor weight	0.03 kg to 300 kg
Maximum rotor diameter	100 mm to 800 mm
Maximum support distance	250 mm to 2100 mm
Rotor shaft diameter range	5 mm to 120 mm
Balancing speed range	400 rpm to 3000 rpm
Drive motor power	0.05 HP to 3 HP
Minimum measurable imbalance	0.01 g to 0.1 g
Imbalance reduction rate	$\geq$95 %
Minimum achievable specific imbalance	0.2 g · mm/kg
Applicable rotor types	Motor rotors, flywheels, impeller body, etc.

Compared with the calculated results, there is a discrepancy of 1.966 g in balance mass of the main disk and 1.849 g for the secondary disk. When at rest, the main disk exhibits a difference of 1.972 g while the secondary disk shows a difference of 1.789 g.

Deviations were observed between the test results of the dynamic balancing machine (e.g., residual unbalance) and the theoretical values. Potential sources of error include installation accuracy, sensor calibration, and bearing clearance. During installation, minor deviations in the blades and disks may compromise geometric symmetry and precise alignment, thereby affecting unbalance measurement. Calibration errors in sensors and environmental factors may also alter sensitivity, leading to inaccuracies in the test results. Excessive bearing clearance might distort vibration signals, further impacting unbalance calculations. Despite these deviations, repeated tests demonstrated consistency with only minor errors, indicating a limited impact on the overall conclusions. However, to ensure reliability, further optimizations are required: improving assembly precision, enhancing sensor accuracy and stability, and strictly controlling environmental conditions. Additional error analysis and refined methodologies will further enhance result accuracy, thereby ensuring the scientific validity and effectiveness of the shot-blasting machine design optimization.

According to the JB/T 3713.2 'Technical Conditions for Double Disc Shot Blasters,' the unbalance should be less than 1.297 g; therefore, reductions were made in both the main disk and secondary disk of the impeller body. While drilling for weight reduction, caution was exercised to avoid excessive loss at specific positions so as not to compromise the structural integrity and strength of the impeller body. Fig. 2 illustrates the modified impeller body, with red circles indicating locations where weight reduction was performed. Subsequent re-testing revealed that after drilling (as depicted in Fig. 3), the main disk exhibited an unbalance of 0.294 g at 288°, while the secondary disk showed an unbalance of 0.316 g at 272°; upon rotation cessation, these values further decreased to 0.272 g and 0.376 g, respectively, all well within the controlled limit of 1.297 g.

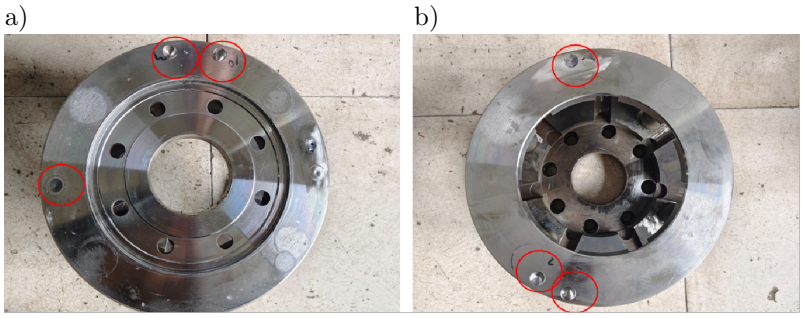

Fig. 2. Evaluation of the primary disk of the impeller body following dynamic balancing (a), examination of the auxiliary disk of the impeller body after dynamic balancing (b).

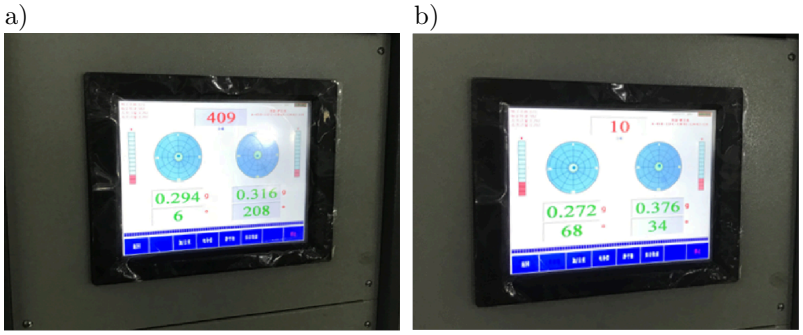

Fig. 3. Residual unbalance of the impeller body during rotation after achieving balance (a), and at rest after achieving balance (b).

The particle velocity of the shot-blasting device was subsequently analyzed using the discrete element method [18–20]. The particle velocity of the shot-blasting device with seven prime-number angular front curved blades reached a maximum value of 75 m/s, with velocity fluctuations within 4 m/s. Furthermore, particles accelerated by the shot-blasting device achieved a relatively stable state after reaching 0.24 s. Through analysis of four other shot-blasting models, it was found that the ejection speed of the eight-uniform front-curved blade is 74 m/s, while for the eight-uniformly distributed straight-blade shot blaster and seven-uniformly distributed straight-blade shot blaster, their ejection speeds were measured at 64 m/s and 69 m/s, respectively. These two types exhibited lower ejection speeds and poorer ejection stability. Similarly, although the seven-uniformly distributed forward-curved blade shot blaster demonstrated a high ejection speed, its stability was also inadequate in comparison. In terms of overall ejection stability among these devices, it can be concluded that the shot-blasting device with seven prime-number angular front-curved blades outperforms the other configurations. Therefore, it is speculated that this particular device will exhibit superior cleaning efficiency during operation.

3. Vibration signal analysis and noise detection of the shot-blasting machine

In order to evaluate the resonance improvement effect and noise optimization of the new shot-blasting device, a comparison was made between the frequency-domain and time-domain signals of the newly designed device and a traditional shot-blasting device. The Hansford's HS-150 acceleration sensor was selected for measuring vibration, with data acquired using the VK701 H model. Vibration data from both devices were collected at a sampling frequency of 10 Ksps, as shown in Fig. 4 and Fig. 5, depicting time-domain analyses before and after op-

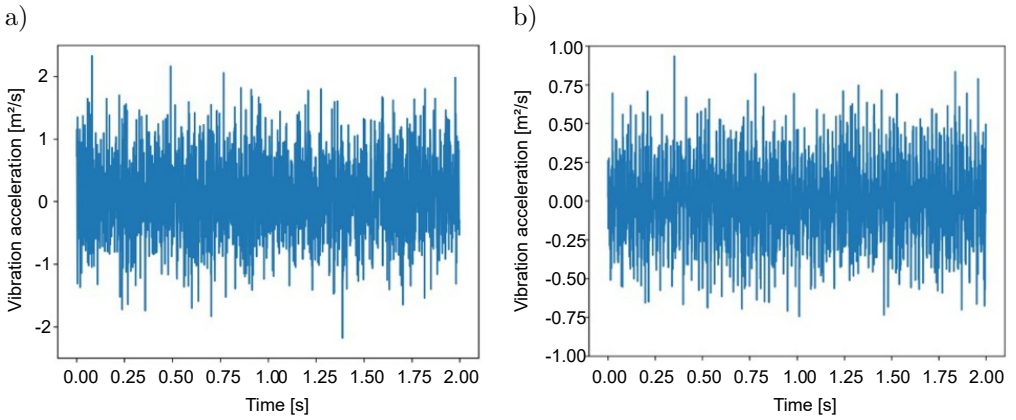

Fig. 4. Time-domain analysis: a) time-domain diagram of position 1 before optimization, b) time-domain diagram of position 2 before optimization.

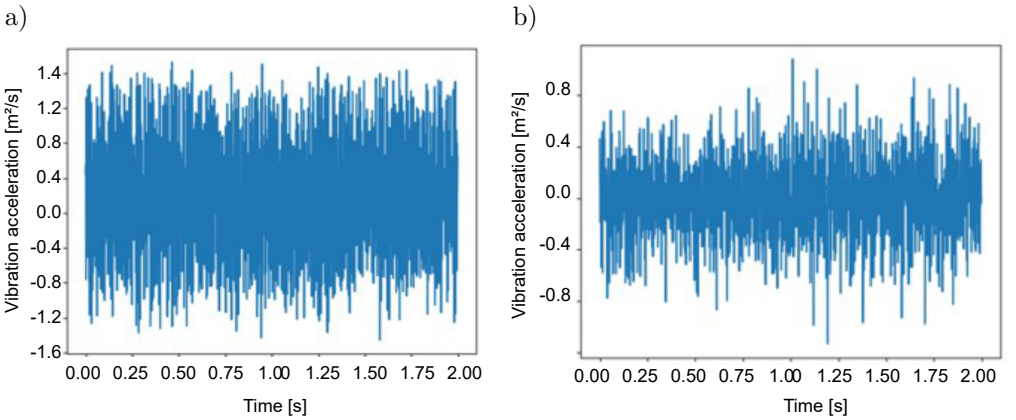

Fig. 5. Time-domain analysis: a) time-domain diagram of position 1 after optimization, b) time-domain diagram of optimized position 2.

timization. Specifically, Fig. 5 presents the vibration acceleration time-domain diagrams of the new shot-blasting device [21–24]. Analysis of the 10 Ksps vibration signal revealed significant improvement in resonance for the Q034ZZ shot blaster: disappearance of the 2nd order component, reduction of amplitude of the 9th order component decreased to approximately 50 % of the fundamental BPF, and overall low amplitude for other frequencies, effectively controlling resonance between the impeller body and motor. Both time-domain and frequency-domain analyses demonstrate a remarkable improvement in the performance of the entire machine [25, 26].

To mitigate the impact of random peaks, vibration intensity was quantified using the root-mean-square (RMS) acceleration within the same 2-seconds window. As depicted in Fig. 4 and Fig. 5, the RMS at position 1 decreased

from $0.800\,\mathrm{m/s^2}$ to $0.467\,\mathrm{m/s^2}$ ($\Delta = 0.333\,\mathrm{m/s^2}$, a reduction of 41.6 %), and at position 2 from $0.283\,\mathrm{m/s^2}$ to $0.217\,\mathrm{m/s^2}$ ($\Delta = 0.067\,\mathrm{m/s^2}$, a reduction of 23.5 %). The reductions in RMS at both measurement points indicate effective suppression of the shot-blasting device's vibration. Thus, the structure designed in accordance with the prime-number/uniform angular-distribution criterion attains a remarkable optimization effect.

In this study, the collected vibration signals are organized into groups, with each group containing 5000 data points. Considering a sampling rate of 10 Ksps, there are a total of 20 groups. Consequently, the fast Fourier transform (FFT) is employed to convert the time-domain signals into frequency-domain signals, as illustrated in Fig. 6 and Fig. 7. To preserve fidelity and comparability with the

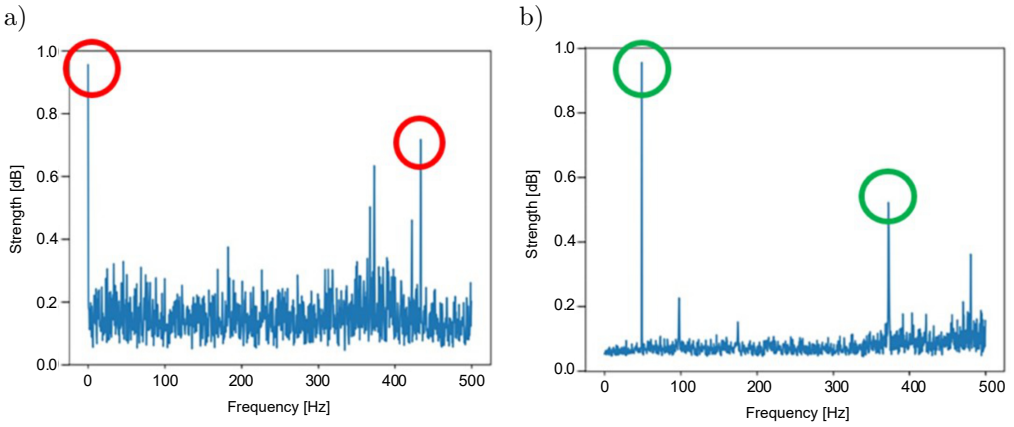

Fig. 6. Frequency domain analysis: a) frequency-domain diagram of the vibration signal at position 1 before optimization, b) frequency-domain diagram of the vibration signal at position 2 before optimization.

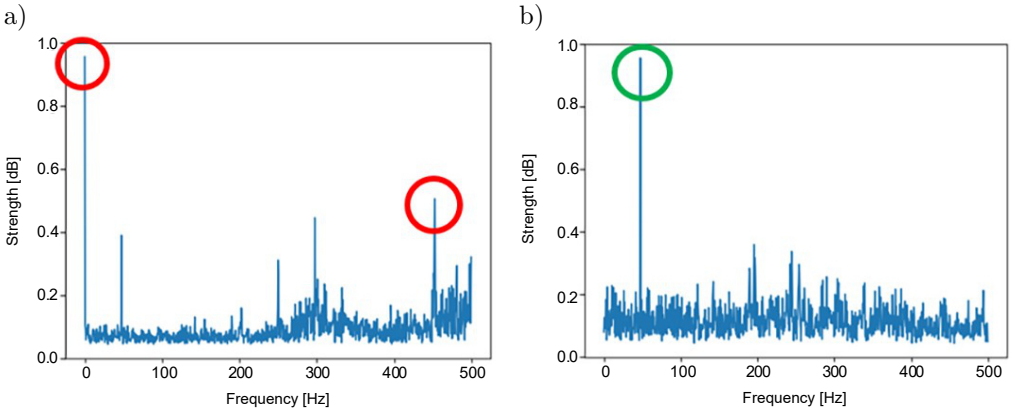

Fig. 7. Frequency-domain analysis: a) frequency-domain diagram of the vibration signal at position 1 after optimization, b) frequency-domain diagram of the vibration signal at position 2 after optimization.

raw measurements, the spectra shown are in their original form, i.e., without additional high-pass filtering or detrending; consequently, the narrow component near 0 Hz in Fig. 6a arises from acquisition-chain offset/slow drift. Moreover, numerous research findings have demonstrated that FFT effectively mitigates data errors; hence, it can be utilized for noise reduction applications in various data-related problems [27–30]. The FFT serves as the foundation for computing the discrete Fourier transform (DFT).

The frequency-domain signals before and after vibration optimization are compared and analyzed. The peaks of the frequency-domain signals before and after optimization are marked with red and green circles, respectively, as depicted in Fig. 6 and Fig. 7. Figure 6a and Fig. 7a present the frequency-domain diagrams at position 1 (radial position) before and after optimization. It can be observed from the diagrams that, under the load state of the shot-blasting machine, the intensity of each blade-passing harmonic order is reduced compared to the second-order blade-passing component. Specifically, the highest value decreases from accounting for 70 % of the fundamental frequency to 50 %, effectively suppressing resonance. On the other hand, Fig. 6b and Fig. 7b depict the frequency-domain diagrams at position 2 (axial position) before and after optimization. It can be seen that each harmonic amplitude improves following optimization with a significant reduction observed in the second-order component – decreasing from representing 50 % of their respective fundamental frequencies to approximately 20 %. Furthermore, in Fig. 7b, it is noteworthy that the other harmonics' highest values account for only 30 % of their corresponding fundamental frequencies indicating a good vibration-reduction effect. In addition, in Fig. 6a, the dominant line occurs at 375 Hz to 380 Hz. With $z = 7$ blades, this line corresponds to the BPF $= zn/60$. Back-calculating the speed gives $n \approx 60 f_{\mathrm{BPF}}/z \approx 3.23$ krpm. Given the frequency resolution used in this study ($\Delta f = 2$ Hz), the resolution-limited uncertainty is about ± 17 rpm. Hence, the peak being higher than the expected 350 Hz at the nominal 3000 rpm is explained by a slightly higher actual speed rather than an analysis artifact. The component near 50 Hz in Fig. 6b originates from mains/electromagnetic coupling and is unrelated to blade orders, whereas the line near 430 Hz in Fig. 6a is a non-integer-order response consistent with a structural or bearing-related mode of the assembly at the measured speed. Both components decrease after optimization, while the BPF-related orders exhibit the largest attenuation.

The optimized impeller structure of the shot blaster has significantly contributed to reducing resonance and minimizing the acceleration value of the vibration signal, as evidenced by the results presented in Fig. 5 and Fig. 7. These findings not only validate the effectiveness of designing the impeller structure based on prime-number/uniform angular distribution criterion for shot blaster blades, but also demonstrate its rationality. This remarkable improve-

ment can be primarily attributed to the seven prime-number angular front-curved blade design, which effectively mitigates resonance and friction between blades, thereby reducing operational vibrations in the shot-blasting machine.

The noise levels of the two shot blasters at 3000 rpm were tested, and the noise levels of the traditional Q034ZZ shot blaster and the newly designed shot blaster based on the blade prime-number/uniform angular distribution criterion were compared. A noise-level meter with a measurement range of 80 dB to 130 dB was used to detect at a distance of one meter to eliminate external interference. The results show that the noise level of the newly designed shot blaster is reduced by 3.7 dB, from 97 dB to 93.3 dB, which proves the effectiveness of the new design in noise reduction.

4. Conclusion

In this paper, a resonance-coupling-reduction-based optimization method was proposed to address the issue of increased vibration in the Q034ZZ shot-blasting machine caused by motor and blade resonance. The geometric limitations of traditional impeller bodies have resulted in scarce optimization methods. This study introduces an innovative prime-number/uniform angular distribution criterion and designs a shot-blasting device with seven prime-number angular front-curved blades based on this principle. The discrete element method was employed to analyze ejection velocity and stability, while drilling the impeller body helped reduce imbalance due to uneven blade distribution. Subsequently, projectile velocity, projectile stability, and vibration signals from the shot-blasting device were explored. It was observed that both the second-order and nine-frequency components exhibit lower amplitude values compared to other frequency multiples, which account for less than 50 % of the fundamental frequency. This represents significant improvement compared to traditional shot-blasting devices, in which such amplitudes exceed 75 %. These findings demonstrate the feasibility of using a seven prime-number angular curved-blade shot-blasting device for vibration and noise reduction purposes. In this experiment, noise measurements were conducted on both the traditional shot-blasting device and the shot-blasting device with seven prime-number angular front-curved blades resulting in a noise reduction from 97 dB (traditional) to 93.3 dB (seven prime-number angular), thus verifying the excellent noise-reduction performance achieved through the design improvements.

Despite these promising results, this study has certain limitations. The optimization method was primarily tested on a single type of shot-blasting machine, and further validation under different configurations and operating conditions is needed. Additionally, although the seven prime-number angular blade design effectively reduces vibration and noise, its impact on other factors, such as en-

ergy efficiency and service life requires further investigation. Future research will address these aspects and extend the methodology to other types of machinery. Nevertheless, the proposed design shows significant promise for applications in industries such as wind power and aerospace. As noise-reduction standards become stringent, the demand for this technology is expected to grow, presenting substantial potential for industrial machinery and environmental protection.

Fundings

This research was funded by Natural Science Foundation of Shandong Province (grant no. ZR2022ME118).

Conflict of interest

The authors declare that they have no known competing financial interests or personal relationships that could have appeared to influence the work reported in this paper.

Authors' contributions

Yong Li: conceptualization, methodology, and writing – original draft preparation. Yaao Di: methodology and writing – review and editing. Wenzheng Dong: validation, resources, and writing – review and editing. Fangxiang Yin: resources and literature survey. Yihao Yin: resources and literature survey. Shanling Han: funding acquisition, writing – review and editing, supervision, and project administration. All authors reviewed and approved the final manuscript.

References

1. Zifeng X., Yan W., Zhihai S., Study on noise reduction of Q400C shot blasting machine [in Chinese], *Modern Manufacturing Technology and Equipment*, **56**(8): 7–8, 2020.
2. Mayers R.A. [Ed.], *Encyclopedia of Physical Science and Technology*, 3rd ed., Academic Press, 2002.
3. Chen W.-K., *Mathematics for Circuits and Filters,* pp. 83–111, CRC Press, Boca Raton, eBook, 2022.
4. Sundararajan D., *Signals and Systems: A Practical Approach*, Springer, Cham, 2022.
5. Sahu O., Das P., Muni M.K., Pradhan N., Basa B., Sahu S.K., Frequency-based crack effect study on beams under free vibration using finite element analysis, *Engineering Transactions*, **72**(1): 95–114, 2024, https://doi.org/10.24423/EngTrans.3166.2024.
6. Zhang X., Yan P., Lu W., Cheng Y., Sun C., Zhu J., Guo W., Cheng X., Frequency spectrum characteristics of blast-induced vibration with electronic detonators in ground

blasting, *Journal of Building Engineering*, **74**: 106892, 2023, https://doi.org/10.1016/j.jobe.2023.106892.

7. Wang Q., Tao T.-J., Jia J., Tian X.-C., Xie C.-J., Analysis of blasting vibration duration considering frequency and energy and its application, *Heliyon*, **10**(12): e33210, 2024, https://doi.org/10.1016/j.heliyon.2024.e33210.

8. Deng Z., Meng J., Deng Y., Ni J., Ye D., Analysis of vibration signals near ground surface during blasting excavation of a tunnel in fractured rock, *Scientific Reports*, **14**: 21909, 2024, https://doi.org/10.1038/s41598-024-73089-1.

9. Guo J., Fei H., Yan Y., Research and advances in the characteristics of blast-induced vibration frequencies, *Buildings*, **15**(6): 892, 2025, https://doi.org/10.3390/buildings15060892.

10. Luo L., Wu Y., Peng Z., Ouyang H., Experimental and numerical study on the noise of uneven-spaced automobile cooling fans [in Chinese], *Noise and Vibration Control*, **41**(5): 175–181, 2021, https://doi.org/10.3969/j.issn.1006-1355.2021.05.028.

11. Zhang Y., Wang S., Pan Y., Zhang T., Jiang Z., Fu X., Research on Optimization design of shot blasting machine blade based on modal analysis [in Chinese], [in:] *2021 Global Reliability and Prognostics and Health Management (PHM-Nanjing)*, 2021, https://doi.org/10.1109/PHM-Nanjing52125.2021.9612963.

12. Wu F., Tang D., Zhao J., Wang B., Luo X., Zhang W., Guo C., Finite element analysis on forward-curve blade of shot blasting machine based on ANSYS [in Chinese], *Mechanical Research & Application*, **28**(03): 27–29, 2015, https://doi.org/10.16576/j.cnki.1007-4414.2015.03.012.

13. Choi D., Kim T., Yang C., Nam J., Park J., Discrete element method and experiments applied to a new impeller blade design for enhanced coverage and uniformity of shot blasting, *Surface and Coatings Technology*, **367**: 262–270, 2019, https://doi.org/10.1016/j.surfcoat.2019.04.008.

14. Zhang D., Liu Y., Wang Z., Analysis of noise by horizontal mobile shot blasting equipment [in Chinese], *Journal of Heilongjiang University of Science*, **2011**(4): 297–300, 2011.

15. Zhou K., Qiao B., Liu M., Gao W., Dai J., Chen X., A novel OPR-free method for blade tip timing based on adaptive variable reference blades, *Aerospace Science and Technology*, **142**(Part B): 108708, 2023, https://doi.org/10.1016/j.ast.2023.108708.

16. Zhang T., Wang S., Yousuf Y.A., Jiang Z., Fang J., Fu X., Men X., Study on the dynamic fatigue performance of shot blasting machine's blades based on modal analysis, *Journal of Physics: Conference Series*, **1948**: 012214, 2021, https://doi.org/10.1088/1742-6596/1948/1/012214.

17. Wang Y., Sun Z., Liu J., Liu M., Zhou Y., Optimization design of centrifugal impeller based on Bezier surface and FFD space grid parameterization, *PLoS ONE*, **19**(11): e0310792, 2024, https://doi.org/10.1371/journal.pone.0310792.

18. Hou L., Yang L.Y., Wang Y.Z., Wang S.R., Kinematics simulation analysis of shots in shot blasting machine based on EDEM, *Applied Mechanics and Materials*, **121**–**126**: 2071–2074, 2011, https://doi.org/10.4028/www.scientific.net/AMM.121-126.2071.

19. Liu Y., Li Q., Kinetic analysis of shot blasting machine with forward curve blades based on EDEM [in Chinese], *Machine Building & Automation*, **46**(06): 130–132+136, 2017, https://doi.org/10.19344/j.cnki.issn1671-5276.2017.06.036.

20. Yan X.Y., Wang S.R., Wen D.S., Wang G.Q., Kinematics simulation analysis of shot blasting projectile based on EDEM, *DEStech Transactions on Engineering and Technology Research*, 2018, https://doi.org/10.12783/dtetr/pmsms2018/24869.

21. Liss M., Martynyuk V., Vibration analysis of shot wheel in abrasive blasting, *MATEC Web Conferenes*, **375**: 02006, 2023, https://doi.org/10.1051/matecconf/202337502006.

22. Yang Z., Fault diagnosis of engine abnormal sound based on vibration analysis [in Chinese], *Special Purpose Vehicle*, **2024**(09): 109–112, 2024, https://doi.org/10.19999/j.cnki.1004-0226.2024.09.027.

23. Fu X., Huang K., Sidiropoulos N.D., Ma W.-K., Nonnegative matrix factorization for signal and data analytics: Identifiability, algorithms, and applications, *IEEE Signal Processing Magazine*, **36**(2): 59–80, 2019, https://doi.org/10.1109/MSP.2018.2877582.

24. Yang J., Shi A., Peng Y., Peng P., Liu J., Interface state-based bound states in continuum and below-continuum-resonance modes with high-Q factors in the rotational periodic system, *Chinese Physics B*, **33**(8): 084206, 2024, https://doi.org/10.1088/1674-1056/ad4630.

25. Lydakis E., Koss H., Brincker R., Amador S.D.R., Data-driven sensor fault diagnosis for vibration-based structural health monitoring under ambient excitation, *Measurement*, **237**: 115232, 2024, https://doi.org/10.1016/j.measurement.2024.115232.

26. Qiu Z., Fan S., Liang H., Liu J., Multimodal fusion fault diagnosis method under noise interference, *Applied Acoustics*, **228**: 110301, 2025, https://doi.org/10.1016/j.apacoust.2024.110301.

27. Shunxi W., Wenjin H., The characteristics and relationships of FT, ZT, DFS, DFT and FFT transformations, *Practical Electronics*, **2015**(01): 121, 2015, https://doi.org/10.16589/j.cnki.cn11-3571/tn.2015.10.240.

28. Runjie W., Wenzhong S., Xianglei L., Zhiyuan L., An adaptive cutoff frequency selection approach for fast Fourier transform method and its application into short-term traffic flow forecasting, *ISPRS International Journal of Geo-Information*, **9**(12): 731, 2020, https://doi.org/10.3390/ijgi9120731.

29. Yang P., Zhou W., Algorithmic analysis towards time-domain extended source waveform inversion, *Pure and Applied Geophysics*, **181**: 2765–2785, 2024, https://doi.org/10.1007/s00024-024-03556-3.

30. Chen Y., Hou L., Lin R., Song J., Ng T.Y., Chen Y., Corrigendum to "A harmonic balance method combined with dimension reduction and FFT for nonlinear dynamic simulation" [Mech. Syst. Signal Process. 221 (2024) 111758], *Mechanical Systems and Signal Processing*, **223**: 111848, 2025, https://doi.org/10.1016/j.ymssp.2024.111848.

Received July 3, 2025; revised September 17, 2025; accepted September 18, 2025; available online December 11, 2025; version of record March 2, 2026; published issue March 30, 2026.